PERGAMON

International Journal of Heat and Mass Transfer 45 (2002) 4631–4641

International Journal of HEAT and MASS TRANSFER

www.elsevier.com/locate/ijhmt

A study of the effect of ultrasonic vibrations on phase-change heat transfer

Y.K. Oh [a], S.H. Park [a], Y.I. Cho [b,*]

[a] Department of Mechanical Engineering, Chosun University, Gwangju, 501-759, South Korea
[b] Department of Mechanical Engineering and Mechanics, Drexel University, Building 3-157, Philadelphia, PA 19104, USA

Received 28 November 2001; received in revised form 16 April 2002

Abstract

The present paper investigates the effect of ultrasonic vibrations on the melting process of a phase-change material (PCM). Furthermore, the present study considers constant heat-flux boundary conditions, whereas much of the previous research had adopted constant wall-temperature conditions. The experimental results revealed that ultrasonic vibrations accompanied the effects like agitation, acoustic streaming, cavitation, and oscillating fluid motion, accelerating the melting process as much as 2.5 times, compared to the rate of natural melting (i.e., the case without ultrasonic vibration). In addition, temperature and Nusselt numbers over time provided conclusive evidence of the important role of the ultrasonic vibrations on the melting phenomena of the PCM.

Keywords: Ultrasonic vibrations; Phase-change heat transfer; Melting

1. Introduction

Solid–liquid phase change (i.e. melting or solidification) occurs in a number of situations of practical interest. Some common examples include the melting of edible oil, metallurgical processes such as casting and welding, and in materials science applications such as crystal growth. Due to the practical importance of the subject, there have been a large number of experimental and numerical studies of melting problems involving phase change [1–9]. Cho and Sunderland [1] investigated heat conduction problems involved in melting and freezing phenomena. Chan et al. [2] developed the theory of melting phenomena based on two-phase region, i.e. solid and liquid regions. Gau and Viskanta [3] measured the melting speed and heat transfer coefficient of a pure metal (Gallium) and obtained a heat-transfer correlation in terms of dimensionless parameters such as Rayleigh, Stefan, and Nusselt numbers. However, these studies [1–3] focused on conduction or natural-convection heat transfer. Other studies [4–8] dealt with the effect of ultrasonic vibrations on the melting process. Hong [9] suggested that ultrasonic vibrations increased the melting rate in the processes applied in chemical and medical industries.

The objective of the present study was to investigate the melting process of a phase-change material (PCM) with ultrasonic vibrations and compare the results with the case without ultrasonic vibrations (natural melting). Furthermore, the study considered constant heat-flux boundary conditions unlike many of the previous investigations, which had adopted constant wall-temperature conditions. Paraffin was selected as the PCM since its thermophysical properties [10] are well established. It is much less expensive and more easily available than hexadecane or tetradecane. Moreover, paraffin is more stable in a phase-change region.

2. Modeling for melting processes

Hong [9] and Ho and Viskanta [11] developed a theoretical analysis based on their two-dimensional

* Corresponding author. Tel.: +1-215-895-2425; fax: +1-215-895-1478.
E-mail address: choyi@drexel.edu (Y.I. Cho).

0017-9310/02/$ - see front matter
PII: S0017-9310(02)00162-X

Nomenclature

h	heat transfer coefficient, kcal/h m^2 °C or W/m^2 K
Δh_f	latent heat of fusion, kJ/kg
f	frequency of acoustic pressure, Hz
g	gravitational acceleration, m/s^2
q''	heat flux, kcal/h m^2 or W/m^2
t	time, h or s
C_p	specific heat of liquid phase, kJ/kg K
H	height of solid paraffin (characteristic height)
K	thermal conductivity of liquid phase, kcal/h m °C or W/m K
T	temperature, °C
Fo	Fourier number (Eq. (6))
Nu	Nusselt number (Eq. (5))
P	period
Pr	Prandtl number, defined as ν/α
Ra	Rayleigh number (Eq. (2))
Ra^*	modified Rayleigh number (Eq. (4))
S	image scale factor
Ste	Stefan number (Eq. (1))
Ste^*	modified Stefan number (Eq. (3))
X	relative horizontal position (see Fig. 1)
Y	relative vertical position (see Fig. 1)
V	velocity vector

Greek symbols

α	thermal diffusivity of liquid phase
β	thermal expansion coefficient
ρ	density of liquid paraffin
ν	kinematic viscosity
τ	normalized time, time/total time consumed to melt PCM

Subscripts

f	fusion
h	heater surface
i	liquid–solid interface
l	liquid
s	solid

models. They presented dimensionless numbers such as Stefan and Rayleigh, respectively.

$$Ste = \frac{C_p(T_h - T_l)}{\Delta h_f} \tag{1}$$

$$Ra = \frac{g\beta(T_h - T_l)H^3 Pr}{\nu^2} \tag{2}$$

In the present study, their model and fundamental equations were partially adopted. Fig. 1 presents a two-dimensional model for the melting problem. In the present study, the wall temperature, T_h and the temperature of liquid, T_l increased until the melting was completed because a constant heat-flux boundary condition was considered. Hence, instead of Stefan and Rayleigh numbers, modified Stefan and modified Rayleigh numbers were used by substituting by $T_h - T_l$ in Eqs. (1) and (2) with $q''H/K$, which are defined respectively as:

$$Ste^* = \frac{C_p q'' H}{K\Delta h_f} \tag{3}$$

$$Ra^* = \frac{g\beta q'' H^4 Pr}{K\nu^2} \tag{4}$$

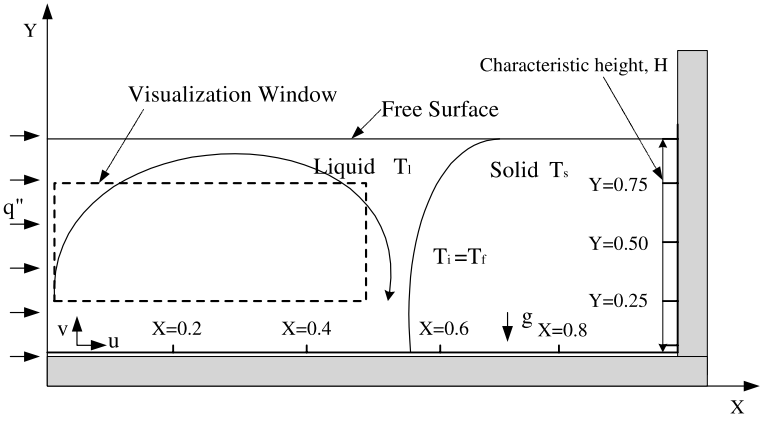

Fig. 1. Two-dimensional model for a melting procedure of a PCM. The rectangular box indicates the area for PIV and flow visualization.

The natural convection in a liquid region could be considered quasi-steady because the solid–liquid interface moved slowly. Experimental evidence [12] indicated that the flow remained entirely laminar in the range of Ra numbers of $10^6 < Ra < 10^9$. Note that the transition to turbulence occurred at Ra numbers greater than 10^9. As Okada [13] and Sparrow et al. [14] reported, Prandtl number did not affect the melting rate for $Pr > 7$ when the modified Rayleigh number was used. In the present study, the value of the Prandtl number was fixed at 40. The modified Rayleigh numbers, Ra^*, had values of 5.80×10^7 and 3.24×10^7, depending on the magnitude of heat flux, during the melting process.

3. Experimental procedure

3.1. Experimental set-up

Paraffin (n-octadecane) with a melting point of 53.2 °C was selected as the PCM, whose properties are listed in Table 1. The test section consisted of a tank and a melting cavity as shown in Fig. 2. The melting cavity filled with paraffin was positioned inside the tank, which was filled with water. The water in the tank was used in order to protect ultrasonic vibrators from electric overload, a phenomenon that could have happened if ultrasonic vibrations had been applied directly to the solid paraffin in the beginning of the melting. In addition, the water medium could minimize heat conduction from the vibrators to the solid paraffin when the vibrators became hot. The melting cavity had inner dimensions of 13 cm × 12.5 cm × 12.5 cm (height × length × width).

Experiments were conducted in a melting cavity as shown in Fig. 2(a). A stainless-steel plate heater was vertically positioned on the left side of the cavity, providing a constant heat-flux regulated by an automatic voltage regulator (Powertek, PAV-500) during the melting process. The back of the heater surface was insulated with a Bakelite plate and fiberglass so that the heat would propagate from the heater surface to the direction of the PCM. In order to check the validity of the insulation, we measured the temperature of the outer side wall of melting cavity before experiments were carried out when the heater plate was sufficiently heated. There were no large deviations (i.e., less than 2 °C), compared to the initial temperature of the melting cavity, confirming that we had an excellent insulation at the backside of the heater. In addition, all four outside walls of the cavity were covered with Styrofoam and fiberglass plate for insulation purposes. Two pairs of ultrasonic vibrators (IBL 4532D, INFITRON Inc, Resonance frequency: 40 ± 1 kHz) are installed at two axial locations, i.e., $X = 0.2$ and $X = 0.8$ as shown in Fig. 2(b).

Table 1
Thermophysical properties of paraffin [15]

Properties	Value
Melting temperature	53.2 °C
Thermal conductivity	0.210 W/m K
Density	863.03 kg/m^3
Specific heat	2873.88 kJ/kg K
Viscosity	0.00028 m^2/s
Heat of fusion	241.60 kJ/kg
Thermal expansion coefficient	0.001

The frequency generated by the ultrasonic frequency generators was monitored by an oscilloscope. Eight chromel–alumel thermocouples of 15-cm length were installed at pre-selected locations ($X = 0.2$, 0.4, 0.6, and 0.8, and $Y = 0.5$; refer Fig. 1 for exact locations) in the melting cavity to measure the temperature distribution of the PCM during the melting process. Each thermocouple was wound in an insulation tape and was sheathed in a stainless-steel tube except at the junction to minimize heat conduction from a connecting thermocouple wire to the PCM. All thermocouples were connected to a data acquisition controller (Yokogawa, Darwin, DA-100), which converted analog signals into digital signals. The temperatures at different positions were continuously recorded on a PC. Fig. 3 shows a schematic diagram for the present data collection set-up. As shown in the Fig. 3, a particle image velocimetry (PIV) was used for the visualization of flow field inside the liquid region of the PCM, and a microphone (H507A, Wilcoxon, Frequency range: 10–100 kHz) was used to measure the pressure distributions in the liquid region when ultrasonic vibrations were applied.

3.2. Experimental procedure

Solid paraffin was first melted, and thus the melting cavity was filled up with melted paraffin. Before experiments were carried out, the liquid paraffin was re-solidified in the melting cavity. After the solidification, some liquid paraffin was also supplied to fill up depressed spots caused by the contraction of the paraffin during the solidification process. Slight irregularities and grooves on the top surface of the paraffin were removed by melting them with hot air. The temperature of the paraffin was initially maintained at room temperature (i.e., 26 °C) at the beginning of each test by keeping the PCM at room temperature for one day. In order to check the repeatability, tests were repeated three times for each heat-flux case. Two different heat fluxes were used in the study:

$$q'' = 9905.1 \text{ kcal/h m}^2 \text{ (The corresponding } Ra^* \text{ was } 5.80 \times 10^7\text{)} = 11511.91 \text{ W/m}^2$$

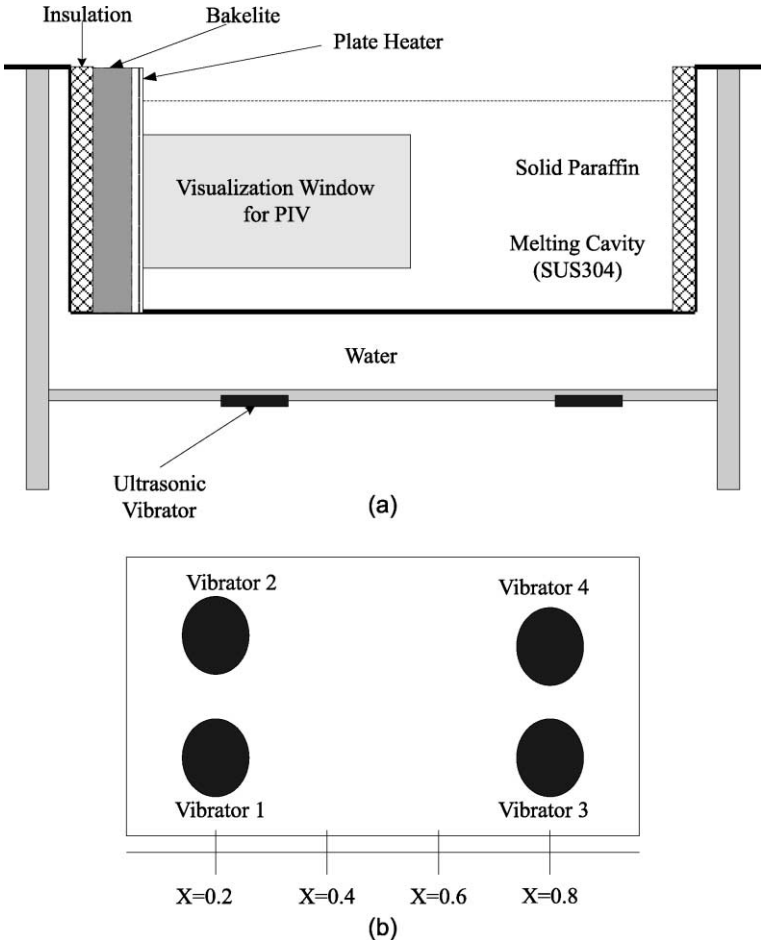

Fig. 2. Schematic diagram of (a) (front view) the present test section consisting of melting cavity and water chamber and (b) (bottom view) the positions of two pairs of ultrasonic vibrators ($X = 0.2$ and 0.8).

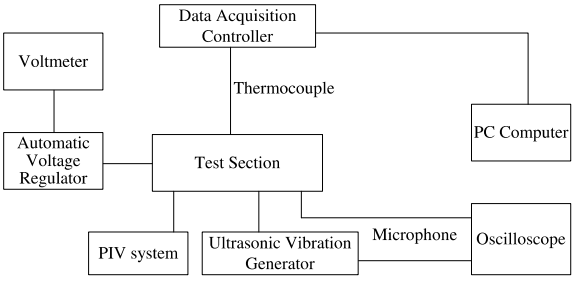

Fig. 3. Schematic diagram for the present experimental set-up.

$$q'' = 5535.2\ \text{kcal/h m}^2\ \text{(The corresponding } Ra^* \text{ was } 3.24 \times 10^7\text{)} = 6433.13\ \text{W/m}^2$$

To obtain a constant heat-flux boundary condition, a plate heater was heated electrically by an automatic voltage regulator, which was designed to maintain a constant output voltage to within ±1%, with an input voltage variation of ±20%. Prior to the experiments, all thermocouples were calibrated with a calibration voltage source. The melting tests were carried out three times under the same condition in order to ensure repeatability and accurate temperature distributions for each experimental case. The largest temperature deviations from the average temperature were about ±5 °C (i.e., ±3.3%) on the heater, and about ±2 °C (i.e., ±2.4%) in the PCM.

Once an experiment began, the heater temperature was measured every one minute during the entire melting process, which took approximately 76–275 min, depending on the magnitude of the heat flux and the use of ultrasonic vibrations. Generally, the physical properties of the paraffin changed when temperature increased above 200 °C because the continuous chains of carbon atoms began to break up at that temperature [15]. Hence, it was necessary to keep the heater temperature below 200 °C. To achieve this, we used the afore-men-

Table 2
Melting time under variable output power levels of ultrasonic vibrator

Heat flux (kcal/h m^2)	Output power level (W)	Melting time (min)
9905.1	70	112
	185	76
	340	59
5535.2	70	164
	185	94
	340	72

tioned two different heat-flux conditions under which the heater surface temperature was kept below 200 °C. In the study, a fixed frequency of 40 kHz and a fixed power level of 185 W were selected for the ultrasonic vibrations but its power level was varied from 70 to 340 W in order to investigate the effect of the strength of the ultrasonic vibrations on the phase-change heat transfer (see Table 2).

4. Results

4.1. Variations of heater-surface temperature

Fig. 4 shows average temperature variations on a heater surface over time under two different experimental conditions: melting without ultrasonic vibrations and melting with ultrasonic vibrations. Heater-surface temperature increased for the first 15 min because the conduction heat transfer from the heater surface to the PCM was predominant in the beginning of melting regardless of the magnitude of the heat flux and melting condition of the PCM. The heater-surface temperature started to increase slowly when natural convection mode was activated. In the case of the melting with the ultrasonic vibrations, sudden temperature increases on the heater surface were observed near the end of melting (see dotted circles marked by arrows in Fig. 4). This can be attributed to the fact that a portion of the heater surface was covered by bubbles formed by the ultrasonic vibrations, a phenomenon which increased the surface temperature for the constant heat-flux boundary condition [16].

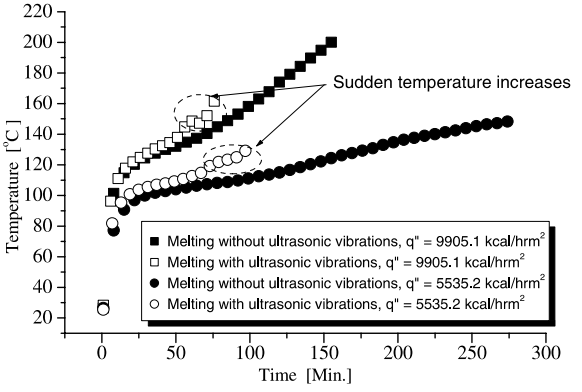

Fig. 4. Variations of heater-surface temperature over time.

The melting times for the case with the ultrasonic vibrations were 76 and 94 min for $q'' = 9905.1$ and 5535.2 kcal/h m^2 respectively, whereas those for the case without the ultrasonic vibrations were 161 and 275 min, respectively. In the present study, the meting time was defined as the time when solid paraffin was transformed into liquid paraffin. It was possible to observe the sate of the paraffin through a transparent cover of the melting cavity insulated by Pyrex glass. The melting time was shortened as much as about 2.5 times compared with that of the natural melting case. The end of the melting coincided with the moment when the heater-surface temperature suddenly increased, suggesting that the factors such as cavitation, acoustic streaming, and thermally oscillating flow motion might have accelerated the melting process after the sudden temperature increase in the heater surface. In summary, the ultrasonic vibrations reduced the melting time, because the vibration significantly accelerated the melting rate.

4.2. Heat transfer coefficient on heater surface

In the early stage of the melting of the PCM, the conduction mode dominated the heat transfer in the melt region, judging from the fact that the molten region appeared to be uniformly parallel to the vertical surface of the heater. As the heating continued, the buoyancy-driven convection in the melt started to develop, pushing the melt upward along the heater surface (see a clockwise large-circular arrow in Fig. 1). The natural convection in the liquid zone continued to intensify as evidenced by the appearance of a nonuniform melting front propagating from a free surface at the top of the cavity (see Fig. 2) to the bottom of the melting cavity. The melt reached the maximum temperature near the free surface and then moved downward at the middle of the cavity along the solid–liquid interface, transporting heat from the heater surface to the solid paraffin. Therefore, it took longer time for the solid paraffin at the bottom of the cavity to melt than that at the top. The onset of the convection should improve the overall heat transfer rate. If the temperature at a liquid–solid interface is assumed to be the same as the fusion temperature of the paraffin, the heat transfer behavior could be expressed in terms of the Nusselt number on the heater surface as follows:

$$Nu = \frac{q''H}{K(T_h - T_f)} \tag{5}$$

where T_h is the heater surface temperature and T_f is the fusion temperature of the PCM. A correlation between the Nusselt number and $Fo\,Ste^*$ is depicted in Fig. 5 for two different heat fluxes and two different experimental conditions, where the Nusselt number divided by $Ra^{*0.25}$ is plotted as a function of a dimensionless parameter $Fo\,Ste^*$. Fourier number, Fo, is a dimensionless time parameter, which represents the ratio of heat transfer by conduction to the energy-storage rate within a material. It is normally defined in the following form:

$$Fo = \frac{Kt}{C_p \rho H^2} = \frac{\alpha t}{H^2} \tag{6}$$

The Fourier number was multiplied by the modified Stefan number, Ste^*, indicating the ratio of sensible heat to latent heat during melting. Consequently, $Fo\,Ste$ could be used as a dimensionless parameter to represent a solid–liquid heat transfer problem [3,11]. The power of 0.25 over Ra^* was generally used in the natural convection problem of PCM.

As shown in Fig. 5, the Nusselt number was very high in the beginning of the melting process and decreased drastically until $Fo\,Ste^*$ reached approximately 0.3×10^5, irrespective of heat fluxes and experimental conditions. After this point (i.e., $Fo\,Ste^* = 0.3 \times 10^5$), the Nusselt number decreased almost linearly with $Fo\,Ste^*$ as the melt zone became wider. The difference in the Nusselt number for each heat-flux case came from the Rayleigh number, which critically depended upon heat flux. That is, the higher the Rayleigh number was, the more active the convection was. Thus, one can conclude that the melting process can be described as a function of Fo, Ste^*, and Ra^* as shown in Fig. 5.

For the case with ultrasonic vibrations, the heat transfer coefficient on the heater surface was further affected by the ultrasonic vibrations, decreasing slightly faster than the case without the ultrasonic vibrations after $Fo\,Ste^*$ reached a value of approximately $1.0–1.3 \times 10^5$. Such points (i.e., $Fo\,Ste^* = 1.0–1.3 \times 10^5$, see Fig. 5) are in good agreement with the points at which the heater-surface temperature suddenly increased; see dotted circles in Fig. 4. Solid paraffin began melting rapidly after this point when the ultrasonic vibrations were applied. Hence, one can conclude that there must be extra effects such as cavitation, acoustic streaming, thermally oscillating flow and strong agitation that enhance the melting rate of the PCM in this period.

In order to examine the effect of the conduction heat transfer on the melting process of the PCM, the effect of the Rayleigh number was excluded, and the Nusselt number was plotted in a range of $0 < Fo\,Ste^* < 0.3 \times 10^5$, in Fig. 6. The Nusselt numbers on the heater surface were almost the same in the beginning of the melting for two different experimental conditions when the Rayleigh number was excluded. The ultrasonic vibrations might have activated some fluid-dynamics phenomena. For example, bubbles produced by the vibrations could affect the heat transfer coefficient on the heat surface, as mentioned earlier (see Fig. 5). That is, the heat transfer coefficient on the heater surface decreased slightly with the ultrasonic vibration compared with the case without the vibration, especially after $Fo\,Ste^*$ reached approximately $1.0–1.3 \times 10^5$ as shown in Fig. 5. However, at the beginning of the melting when the conduction mode dominated over the convection mode, the heat transfer coefficients on the heater surface were almost identical for both cases (with and without the vibrations) because fluid-dynamics phenomena were not activated in spite of applying the ultrasonic vibrations during this period. Consequently, one can conclude that the ultrasonic vibrations did not make much

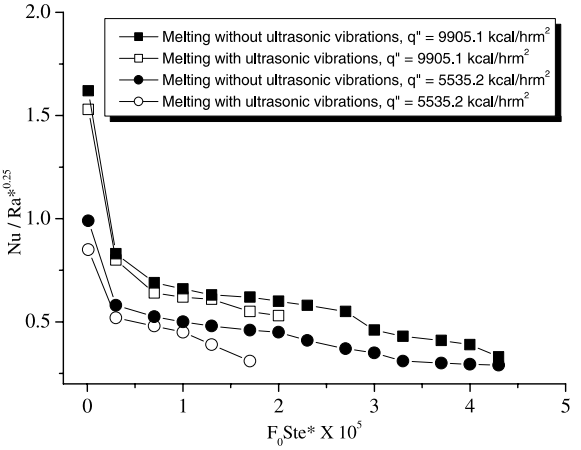

Fig. 5. Nusselt variations on a heater surface with respect to $Fo\,Ste^*$.

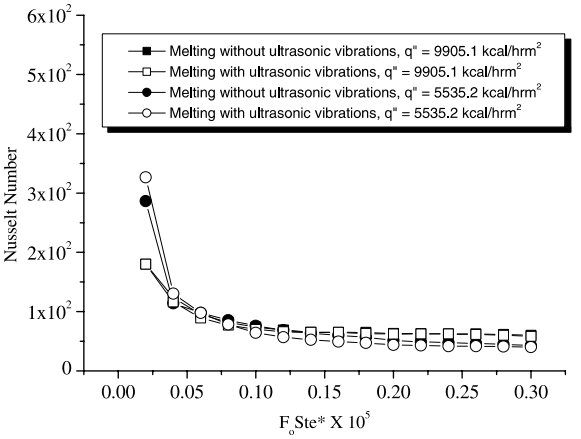

Fig. 6. Nusselt number variations on a heater surface for $Fo\,Ste^* < 0.3$, i.e., during the initial period of melting.

impact on the heat transfer while the conduction mode dominated (i.e., for $FoSte^* < 0.3 \times 10^5$). In short, the ultrasonic vibrations did not increase the heat transfer coefficient on the heater surface, but accelerated the melting rate of the PCM. Next, we will discuss how the ultrasonic vibration could accelerate the melting of the PCM even when the heat transfer coefficient did not increase on the heater surface.

5. Discussions

5.1. Augmentation of heat transfer in the liquid region of PCM

Although the ultrasonic vibration greatly affected the melting rate (see Fig. 4), it did not improve the heat transfer coefficient on the heater surface (see Fig. 5). It is speculated that the heat transfer coefficient on the heater surface is mostly determined by the heater-surface temperature. Therefore, it is necessary to investigate the temperature history of the PCM in order to find what accelerated the melting rate of the PCM. Fig. 7 shows the temperature history of the PCM at $X = 0.2$ and $Y = 0.5$ against normalized time, τ, for two different experimental conditions. The normalized time was obtained by dividing time by the total time consumed to melt the PCM completely. The temperature of the PCM was lower by 15–20 °C for the case of the ultrasonic vibrations than the case without the vibrations. The temperature history of the PCM at other locations also showed similar trends. In short, the ultrasonic vibrations increased the heat transfer coefficient in the liquid as manifested by decreased PCM temperatures. Factors to enhance the heat transfer coefficient in the liquid by the ultrasonic vibrations are discussed next:

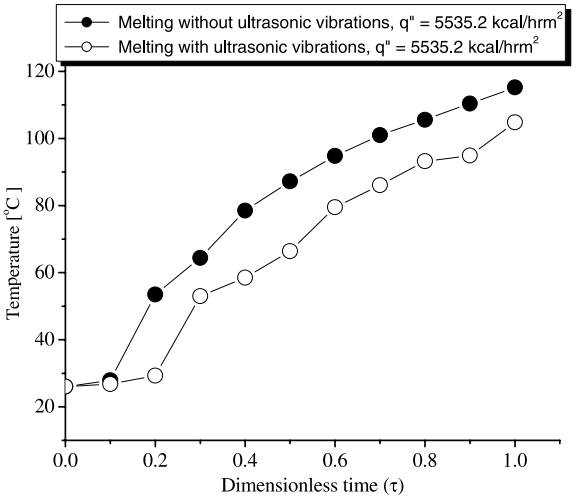

Fig. 7. Temperature history of PCM measured at $X = 0.2$ and $Y = 0.5$ against normalized time (τ).

5.1.1. Acoustic streaming

The application of ultrasound in a medium may cause the flow velocity of the medium to increase: an effect known as acoustic streaming [17,18]. In the present study, the application of ultrasonic vibrations to the PCM liquid were found to induce acoustic streaming, a phenomenon which was observed using a particle image velocimetry (PIV, Powerview^{TM}, TSI, 6000 series, Image resolution: 640×480 pixel, Time resolution: 1/60 s). Actually, acoustic streaming results from the attenuation of an acoustic wave in liquid. The acoustic streaming was shown to enhance both thermal convective streaming and mass transport, where convective transport was superimposed on diffusive transport [19]. In the present study, the induced upward flow caused by acoustic streaming was measured using the PIV for the case of the ultrasonic vibration with a heat flux of 5535.2 kcal/h m^2 and shown in Fig. 8(a). On the contrary, flow vectors induced by the natural convection were shown in Fig. 8(b). Two camera frames from the PIV were processed to find the velocity vector map of the flow field. This involved dividing the camera frames into small areas called interrogation regions. In each interrogation region, the displacement of groups of particles between the two frames, dx, was measured using a correlation technique (i.e., FFT algorithms). The illumination time interval, dt, was obtained from an illumination source. Hence, the velocity vector, V, was calculated as:

$$V = S\frac{\mathrm{d}x}{\mathrm{d}t} \tag{7}$$

where S was an image scale factor for the implementation between CCD camera and measurements area. Strong acoustic streaming with a mean velocity of 3.6 cm/s was found near the ultrasonic transducers.

5.1.2. Cavitation

Cavitation is a result of acoustic waves introduced in the PCM liquid by means of a series of transducers mounted to the test enclosure. The acoustic wave emitted from the transducers travels throughout the enclosure and creates waves of compression and expansion in the liquid. In the compression wave, the molecules of the liquid are compressed together tightly. Conversely, in the expansion wave, the molecules are pulled apart rapidly. The expansion is so dramatic that the molecules are ripped apart, creating microscopic bubbles. The bubbles contain a partial vacuum while they exist in the liquid phase of the PCM. As the pressure around the bubbles increases, the fluid around the bubble rushes in, collapsing the bubble very rapidly. When this occurs, induced flow (acoustic streaming) is created that may travel at a very high propagation rate [20].

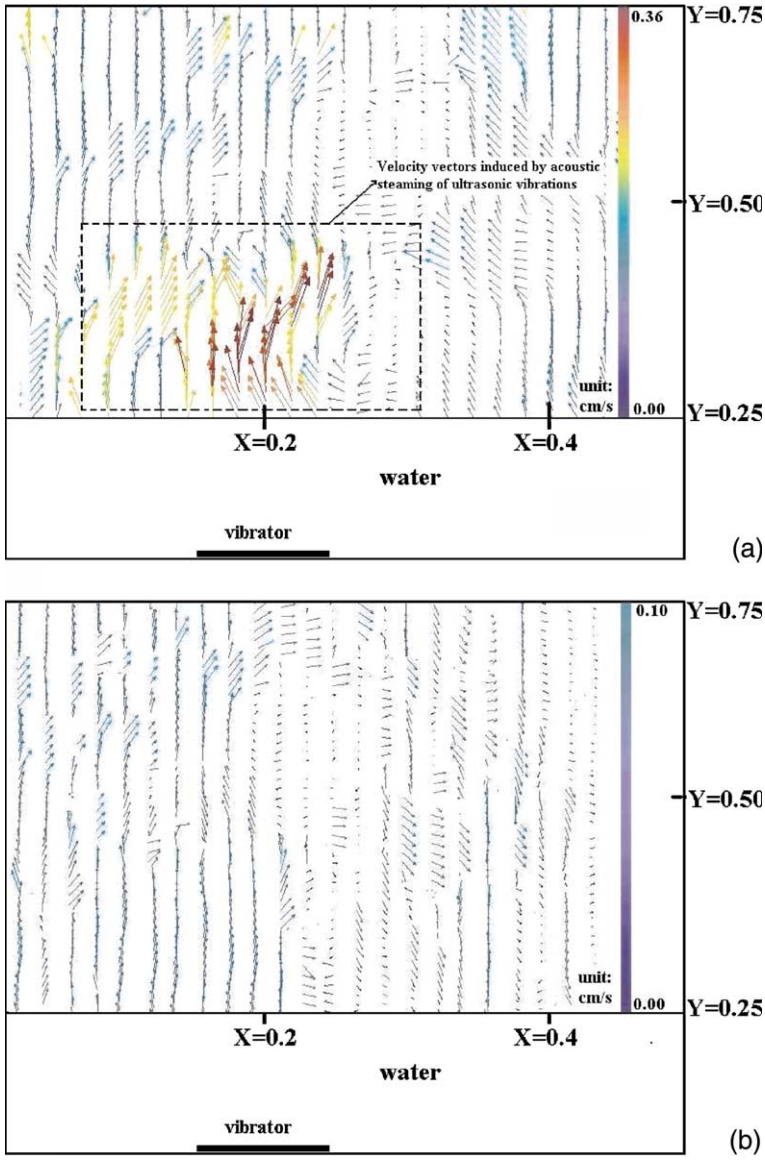

Fig. 8. Comparison of velocity vectors for two cases: (a) two-dimensional velocity profiles induced by acoustic streaming of ultrasonic vibrations measured at a visualization window indicated in Fig. 2 and (b) induced by the natural convection measured at the visualization window.

Actually, the acoustic pressure amplitude was observed at $X = 0.2$ and $Y = 0.5$ using a microphone for the liquid and shown in Fig. 9, where the X-axis was a triggered time at 20 μs per division at oscilloscope (Tektronics, TDS 630C, 500 MHz) axis and the Y-axis was an input signal converted to voltage (5.0 mV per division). All peaks were symmetrical to the X-axis in actual view, but they seemed to be irregular because it was a time-dependant snap shot. When the points of the peaks are connected and lined, we can get compression and expansion cycles of an acoustic wave. India et al. [21] reported that the maximum acoustic pressure amplitude was approximately 1×10^5 Pa.

In order to determine the frequency of the acoustic pressure produced by the ultrasonic vibration in the study, the horizontal scale (time per division) of the waveform varied from 20 μs in Fig. 9 to 5 μs in Fig. 10 (bottom half of the figure). Note that the frequency of acoustic pressure can be obtained in the following form:

$$f = \frac{1}{P}\ [\mathrm{Hz}] \tag{8}$$

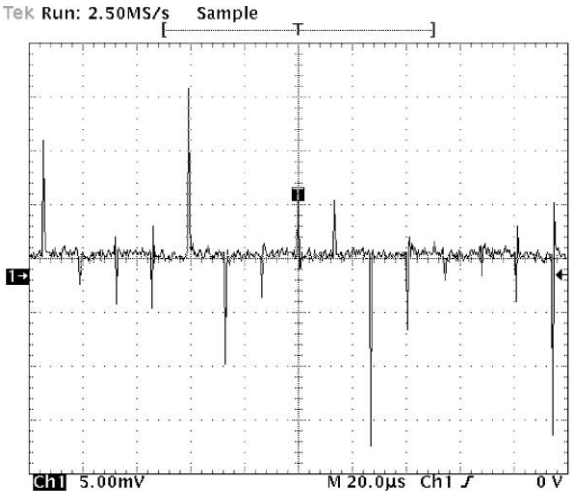

Fig. 9. Waveform of acoustic pressure amplitude at 20 μs per division.

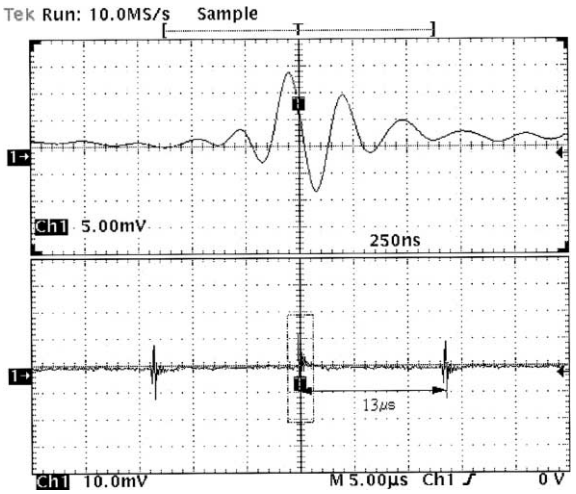

Fig. 10. Acoustic pressure amplitude at 5 μs per division (bottom graph) and enlarged pressure amplitude at 250 ns per division (top graph).

where P is a period of the wave. As shown in Fig. 10 (bottom half of the figure), the acoustic pressure repeated every 13 μs, giving the value of the period of P equal to 13 μs. Therefore, the frequency of the acoustic pressure was estimated to be about 77 kHz. The amplitude of the acoustic pressure was enlarged in Fig. 10 (top half of the figure) by reducing the horizontal scale to 250 ns per division. Some pressure fluctuations were observed in the enlarged signal of the acoustic pressure. It is speculated that such fluctuations were caused by the collapse of cavitation and the acoustic streaming, producing a thermally oscillating flow to be discussed next. Actually, it was reported that the collapse of cavitation produced the necessary agitation energy (i.e., the removal force) and the acoustic pressure fluctuation around fluid [23].

5.1.3. Thermally oscillating flow

Acoustic streaming with cavitation can generate thermal convective streaming, causing an intense fluid motion. The acoustic streaming and cavitation effects seem to increase the melting speed of the PCM. Fig. 11 shows two flow fields captured by an infrared thermal camera (Thermovision® 900, AGEMA, Temperature range $= -10$ to 500 °C, accuracy $= \pm 1$ °C): one with the ultrasonic vibration and the other without it. The flow for the case without the vibration shows a number of horizontal lines from red (liquid PCM) to dark blue (solid PCM), indicating the traditional natural melting mode. When the ultrasonic vibration was applied, one could not see the large number of the horizontal lines any more, suggesting that the flow instability caused by the vibration must have destroyed the diffusion-dominant melting mode. Instead, a large cell appears to exit in the middle of the melting cavity with a dark blue vertical line in the lower left side (about one-quarter distance from the heating surface). We refer to such a

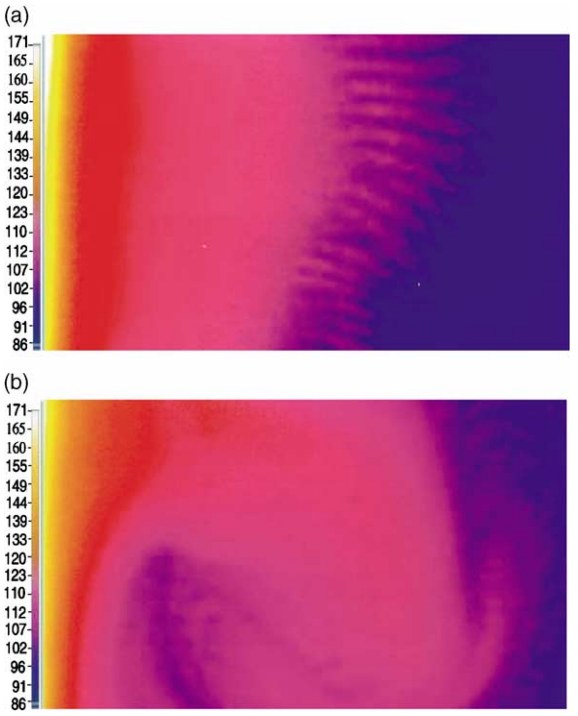

Fig. 11. Comparison of flow fields for two cases: (a) melting without ultrasonic vibrations and (b) with the vibrations. The development of thermally oscillating flow by ultrasonic vibrations is shown in (b).

cell as a thermally oscillating flow driven by the ultrasonic vibration. The oscillating fluid motion was closely connected with the agitation and acoustic streaming initiated by the ultrasonic vibrations. Oscillating fluid motion became intensified as the effects of the acoustic streaming increased. A similar observation was reported by Ha [22].

5.2. Comparison of total consumed electricity for two experimental conditions

Hong [9] reported that a frequency of up to 55 kHz could reduce the melting time and that there was no further improvement of the melting speed beyond that frequency. However, most ultrasonic devices like ultrasonic cleaners and ultrasonic humidifiers use output power variations instead of frequency variations because it is not easy to vary the frequency with a given frequency generator. Hence, the output power level at a frequency generator was adjusted to investigate the effect of the power level of the ultrasonic vibrations on melting phenomena in the present study. Table 2 shows the melting times when the output power levels varied from 70 to 340 W. The higher the output power level was, the faster the melting speed was. The total consumed electricity was also measured for the following two cases: melting with a heater only, and melting with both heater and ultrasonic vibrations. The electric power consumed by the four vibrators (see Fig. 2(b)) was determined by the power supplier of an ultrasonic vibration generator. As shown in Table 3, the total consumed electricity for the case with a heater and ultrasonic vibrations was almost the same as that for the case with a heater only. However, in the present study, ultrasonic vibrations were transmitted through water as shown in Fig. 2. Therefore, the energy saved was negligibly small. However, energy could have been saved by using ultrasonic vibrations by directly applying ultrasonic vibrations to the PCM and turning ultrasonic transducers on only when the solid PCM begins to melt to liquid, since the ultrasonic vibrations participate actively only after the solid PCM changes to a liquid phase.

Table 3
Comparison of the total consumed electricity for a melting process

Heat flux (kcal/h m^2)	Melting time (min)	Heater (Wh)	Ultrasonic vibration generator (Wh)	Total consumed electricity (Wh)
9905.1	161	448.1	–	448.1[a]
	76	211.5	–	445.9[b]
5535.2	275	444.6	–	444.6[a]
	94	152.0	–	441.8[b]

[a] Melting with a heater.
[b] Melting with a heater and ultrasonic vibrations.

6. Conclusion

The melting process in the melting cavity with a heated vertical wall was studied under two experimental conditions: natural melting (i.e., without ultrasonic vibrations) and melting with ultrasonic vibrations. Ultrasonic vibrations accelerated the melting process 2.5 times, compared with the case of the natural melting. This can be attributed to cavitation, acoustic streaming, and thermally oscillating flow initiated by the ultrasonic vibration. Furthermore, energy can be saved compared to the natural melting by properly applying the ultrasonic vibrations.

Acknowledgements

This study was supported in part by a research fund from Chosun University 2000.

References

[1] S.H. Cho, J.E. Sunderland, Heat conduction problems with melting or freezing, J. Heat Transfer 6 (1969) 125–131.
[2] S.H. Chan, D.H. Cho, G. Kocamus-tafaogullari, Melting and solidification with internal radiative transfer, Int. J. Heat Mass Transfer 26 (4) (1983) 621–630.
[3] C. Gau, R. Viskanta, Melting and solidification of a pure metal on a vertical wall, J. Heat Transfer 108 (1986) 204–209.
[4] R. Lemlich, Effect of vibration on natural convective heat transfer, Ind. Engng. Chem. 47 (6) (1955) 121–127.
[5] M.B. Larson, A.L. London, A study of the effect of ultimate vibrations on convective heat transfer to liquids, ASME 62-HT-44 (1962) 62–68.
[6] M.N. Topp, P. Eisenklam, Industrial and medical uses of ultrasonic atomizers, Ultrasonics 48 (1972) 127–132.
[7] H.V. Fsairbanks, Influence of ultrasound upon heat transfer systems, Ultrason. Symp. 1 (1979) 384–389.
[8] F.B. West, A.T. Taylor, The effect of pulsations on heat transfer, Chem. Eng. Progr. 48 (1) (1952) 208–214.
[9] J.S. Hong, Experimental Study of Melting Phenomena with and without ultrasonic vibrations, M.S. Thesis, University Illinois, Chicago, 1988.
[10] J.H. Lee, C.J. Um, An experimental study on the ultrasonic influence for melting the paraffin with solid particles, Proc. SACREK 2 (1999) 285–290.
[11] C.J. Ho, R. Viskanta, Heat-transfer during melting from the isothermal vertical wall, J. Heat Transfer 108 (1986) 204–209.
[12] A. Gadgil, D. Gobin, Analysis of two-dimensional melting in rectangular enclosures in presence of convection, Trans. ASME 106 (1984) 20–26.

[13] M. Okada, Analysis of heat transfer during melting from a vertical wall, Int. J. Heat Mass Transfer 27 (11) (1984) 2057–2066.
[14] E.M. Sparrow, S.V. Patankar, S. Ramadhyani, Analysis of melting in the presence of natural convection in the melt region, ASME J. Heat Transfer 99 (4) (1977) 520–526.
[15] C.S. Hong, Studies on Heat Storing and Retrieving Characteristics in a Paraffin-Filled Horizontal Circular Tube, Ph.D. Thesis, Seoul National University, 1990.
[16] J.G. Kirby, R.Stainforth, L.H. Kinnier, A Visual Study of Forced Convective Boiling. Part II: Flow Patterns and Burnout for a Round Test Section, AEEW-R506, 1967.
[17] S.B. Barnett, Ultrasound Med. Biol. 2 (suppl. 1) (1998) 20–24.
[18] M. Raffel, C.E. Willert, J. Kompenhans, Particle Image Velocitmerty, A Particle Guide, Springer, Berlin, 1998.
[19] V. Frenkel, R. Gurka, A. Liberzon, U. Shavit, Preliminary Investigations of ultrasonic induced acoustic streaming using particle image velocimetry, Ultrasoincs 39 (2001) 153–156.
[20] J. Hilgert, Ultrasonic Cleaning Primer, BRANSON technical report, USA, 1998, pp. 2–6.
[21] T. India, X. Zhang, A. Yabe, Active control of phase change from supercooled water to ice by ultrasonic vibration 1, Int. J. Heat Mass Transfer 44 (2001) 4523–4531.
[22] M.Y. Ha, A theoretical study on the acoustically driven oscillating flow around small spherical particles, KSME Int. J. 6 (1) (1992) 49–57.
[23] Sami Awad, Ultrasonic Caviations and Precision Cleaning, CREST ULTRASONICS technical report, USA, 1996.